Harmonic Signature-Based One-Class Classifier for Islanding Detection in Microgrids

Mazaher Karimi, *Senior Member, IEEE*, Mohammad Farshad, Rasoul Azizipanah-Abarghooee, *Senior Member, IEEE*, and Kimmo Kauhaniemi, *Member, IEEE*

***Abstract*—This article presents a new passive islanding detection technique in MGs that uses locally measured voltage signals at the PoC of DERs. The proposed method distinguishes islanding events from normal/non-islanding conditions by utilizing superimposed harmonic spectra extracted through a full-cycle discrete Fourier transform. Our solution utilizes a machine-learning-based one-class classifier to define and adjust thresholds for full harmonic spectra. Unlike other methods, our approach does not require data synchronization or communication infrastructure, nor does it suffer from common errors that often arise in current transformers. Moreover, our design is compatible with distributed and decentralized control strategies, as it relies solely on local voltage measurements at the PoC. Another advantage of this method is its low sampling frequency requirement, in the range of 1 kHz, making it cost-effective and implementable in most existing systems. In a comprehensive evaluation of a typical MG test system that included synchronous and inverter-based DERs, the proposed scheme demonstrated exceptional performance. Specifically, the scheme was able to detect 99.06% of different islanding events within the training range, with a detection time of just 10 to 21 ms. Additionally, the scheme remained 100% stable during various normal conditions, short-circuit faults, load changes, voltage changes, capacitor switching, and frequency changes.**

***Index Terms*—Discrete Fourier transforms (DFTs), harmonic analysis, islanding, machine learning, microgrids (MGs), pattern classification.**

Nomenclature

δ	Squared distance.
δ_{thr}	Threshold value.
C_j^*	Centroid of the *j*th optimal cluster.
k	Number of clusters.
T_i	*i*th target training pattern.
M	Number of training patterns.
f_b	System's fundamental frequency.
f_s	System's sampling frequency.
FN_V	Number of times the classifier has failed to detect islanding events.
FP_V	Number of times the classifier has mal-operated under normal/non-islanding indicates conditions.
N_V	Total number of validation signals.
VL	Validation loss in percent.
P_{grid}	Active power injected from the utility grid.
Q_{grid}	Reactive power injected from the utility grid.

Abbreviations

DER	Distributed energy resource.
DFT	Discrete Fourier transform.
DSO	Distribution system operators.
k-MDD	*k*-means data description.
MG	Microgrid.
NDZ	Non-detection zone.
PCC	Point of common coupling.
PoC	Point of connection of DER.
PV	Photovoltaic.
THD	Total harmonic distortion.

I. Introduction

THE integration of DERs into active distribution networks, such as MGs, offers many benefits, including improved reliability and power quality. However, it also presents several challenges, one of which is inadvertent islanding. Islanding occurs when DERs, such as wind turbines and PV units, supply power to a portion of the MG that becomes electrically disconnected from the upstream grid [1]. It is critical to detect islanding within a specific time to prevent power quality degradation and ensure the safety of DERs, utility personnel, repair crews, and customers [2], [3]. According to IEEE 1547-2018 standard, there are two types of islands: unintentional and intentional. An intentional island is a planned event, while an unintentional island is unplanned. Regardless of the type, IEEE standard 1547 and UL 1741 require islanding detection within 2 s of an islanding event [4], [5], [6]. Thus, a fast and secure islanding detection method is an essential requirement for MGs, as distribution system operators must manage DER controllers in both islanding and non-islanding conditions.

Islanding detection techniques can be divided into remote and local schemes. Remote methods are based on the communication infrastructure and involve monitoring the status of the circuit

Manuscript received 4 November 2022; revised 24 February 2023; accepted 18 May 2023. This work was supported in part by the University of Vaasa under the CIRP-5G research project with financial support provided by Business Finland under Grant 6937/31/2021, in part by SolarX research project under Grant 6844/31/2018, and in part by the research project is highly acknowledged. *(Corresponding author: Mazaher Karimi.)*

Mazaher Karimi and Kimmo Kauhaniemi are with the School of Technology and Innovations, University of Vaasa, FI-65200 Vaasa, Finland (e-mail: mazaher.karimi@uwasa.fi; kimmo.kauhaniemi@uwasa.fi).

Mohammad Farshad is with the Department of Electrical Engineering, Faculty of Basic Sciences and Engineering, Gonbad Kavous University, Gonbad Kavous 49717-99151, Iran (e-mail: farshad@gonbad.ac.ir).

Rasoul Azizipanah-Abarghooee is with the Rina Tech U.K. Ltd., M1 3LD Manchester, U.K. (e-mail: razizipanah@mail.com).

Digital Object Identifier 10.1109/JSYST.2023.3279389

breaker at the PCC [7]. While the most significant advantage of remote methods is their ability to eliminate NDZs, they are not suitable for small-scale DER installations due to the high costs of communication infrastructure. On the other hand, a local method is also required as a backup in case of loss of data packets. Local methods can be categorized as passive, active, and hybrid approaches [8], [9], [10], [11], [12], [13].

1) Passive methods are easy to deploy and accurate enough during large load-generation mismatches. However, they malfunction when the PCC's mismatch is less than the NDZ. This would give wrong discrimination between islanding and non-islanding events [8], [10], [11], [12].
2) Active methods are introduced to enhance the NDZ by injecting small disturbances into the system parameters like voltage, current, impedance, etc., in terms of amplitude and phase angle. However, this may cause power quality issues and increase detection time [4], [13], [14], [15], [16].
3) Hybrid methods are also introduced to overcome the drawbacks of the passive and active methods [17], [18], [19]. The active method's disturbance is simulated, while the suspicious islanding portion of the MG is detected by the passive method. The complexity and threshold adjustment are the main challenges in this context.

In order to address the above-noticed limitations, different signal-processing techniques have been suggested to extract the system signature features [9], [14], [17], [20]. For example, the wavelet transform can analyze different scenarios by breaking down the time-domain signal into several frequency levels [21]. However, it would cause adverse outcomes for noise-contained signals. Recent studies have acknowledged the usefulness of harmonic information contained in voltage signals for islanding detection [22], [23], [24]. However, analyzing the class of disturbance only with the extracted features requires threshold settings, which is problematic. Hence, to avoid the difficulty of determining multidimensional threshold values, each of these studies [22], [23], [24] has considered only a certain parameter of harmonic information contained in voltage signals and ignored the rest. It should be noted that the signal processing approach can be combined with an intelligent tool like the artificial neural network [25], support vector machine [26], and deep neural network [27] to overcome such difficulty since they can easily deal with multidimensional input feature vectors. However, the simplicity of the calculations should be taken into account to facilitate the real-time implementation of the islanding detection scheme.

An innovative passive islanding detection technique is designed in this article to overcome the shortcomings of the previously mentioned methods, using signal processing and machine-learning approaches. The superimposed harmonic spectra are considered the decision-making input features. In order to extract these features, the full-cycle DFT is performed on the voltage signals locally sampled at the PoC of DERs at a low rate of 1 kHz, which is compatible with the measuring rates specified by the IEC 61850 Sampled Value standard. A machine-learning-based one-class classifier is utilized to decide based on the input features. The employed classifier's computational efficiency and the measured signals' low sampling frequency facilitate real-time implementation. Using the full harmonic spectra in this proposed method improves its comprehensiveness and retains the information required for islanding detection. Another advantage of the proposed method, which sets it apart from the existing literature, is that using the superimposed components significantly reduces the effect of permanent harmonic sources in distribution networks. Furthermore, using only local voltage measurements at the PoC ensures the proposed method is immune to current transformer errors and communication channel failures. Therefore, the proposed method can be implemented compatibly with distributed and decentralized control strategies and at a low cost in most existing systems.

The rest of the article is organized as follows: Section II explains the harmonic signature based on the DFT. Section III presents the proposed islanding detection technique using a machine-learning-based one-class classifier. Section IV evaluates the proposed islanding detection technique's accuracy and robustness in a typical MG, including synchronous and inverter-based generations. Finally, Section V discusses the findings and conclusions of the article.

II. Harmonic Signature

The literature [22], [23], [24] suggests that the harmonic content of the voltage signal can be used to detect islanding events. Nevertheless, previous studies have focused on using a specific harmonic order (e.g., fifth voltage harmonic magnitude in [22]) or a collective parameter (e.g., the selected harmonic distortion in [23] and the THD in [24]) compared to threshold values.

In this article, the full harmonic spectrum of each phase voltage is considered in terms of the selected sampling frequency to increase comprehensiveness and retain helpful information. The harmonic spectrum can be extracted by applying the full-cycle DFT to the sampled voltage signal. The presence of devices with different harmonic characteristics in distribution networks poses one of the challenges that may affect the performance of the harmonic signature-based islanding detection methods [22]. In order to tackle this issue, the superimposed voltage harmonic spectrum is calculated as shown in Fig. 1. It is clear-cut that at each moment, a data-window is taken, including the last two cycles (i.e., for 50 Hz, 40 ms) of each phase voltage signal, and the first cycle's harmonic spectrum is subtracted from the second one. Based on this procedure, the superimposed components will be near zero if the harmonic content remains almost unchanged. This procedure helps to reduce the effect of permanent harmonic sources in steady-state conditions.

Fig. 2 presents a simple system model that complies with the IEEE 1547 test frame [5]. It includes synchronous and PV-based DERs. The three phases' voltage signals are measured at the PoC of PV with a sampling frequency of 1 kHz. The following events are simulated in which P_{grid} and Q_{grid} stand for the active and reactive powers injected by the utility grid, respectively.

1) Event 1—Islanding when $P_{\text{grid}} = 0.585$ MW and $Q_{\text{grid}} = -0.423$ Mvar.

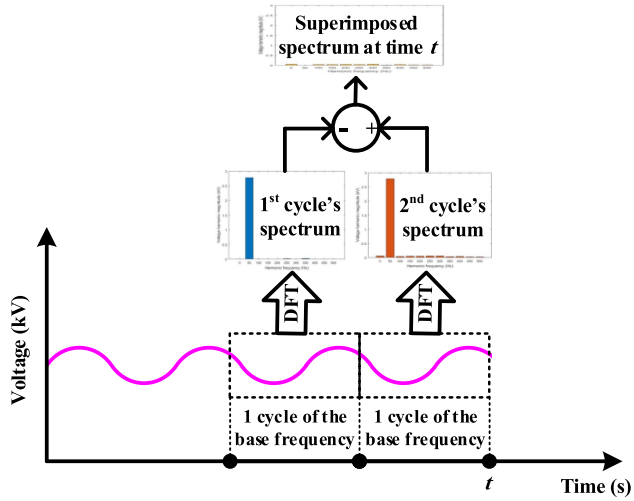

Fig. 1. Calculation of the superimposed voltage harmonic spectrum.

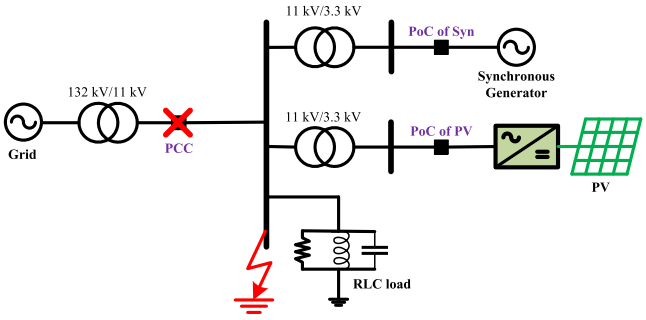

Fig. 2. Simple system modeled compliantly with the IEEE 1547 test frame.

2) Event 2—Islanding when $P_{\text{grid}} = 0.811$ MW and $Q_{\text{grid}} = -0.439$ Mvar.
3) Event 3—Solid phase a-to-ground short-circuit fault when $P_{\text{grid}} = 0.585$ MW and $Q_{\text{grid}} = -0.423$ Mvar.
4) Event 4—Sudden connection of an inductive load with 0.45 MW active power and 0.45 Mvar reactive power when $P_{\text{grid}} = 0.585$ MW and $Q_{\text{grid}} = -0.423$ Mvar.
5) Event 5—A temporary increase in the grid's voltage by 6% when $P_{\text{grid}} = 0.585$ MW and $Q_{\text{grid}} = -0.423$ Mvar.

For each event, the superimposed voltage harmonic spectrum is calculated for phase a, considering a data-window comprising of one cycle before and one cycle after the event occurrence instant.

Fig. 3 shows the superimposed spectra at the time of the first and second islanding events (i.e., events 1 and 2). In addition, Fig. 4 provides the same information for the remaining non-islanding events (i.e., events 3 to 5). As can be seen, the superimposed harmonic spectra of Fig. 3(a) and (b) obtained for the islanding events are significantly identical, while they are dissimilar to those presented in Fig. 4 for the non-islanding events.

In short, according to the above analysis results, the superimposed voltage harmonic spectra can help islanding detection if they are appropriately utilized within an efficient scheme. It

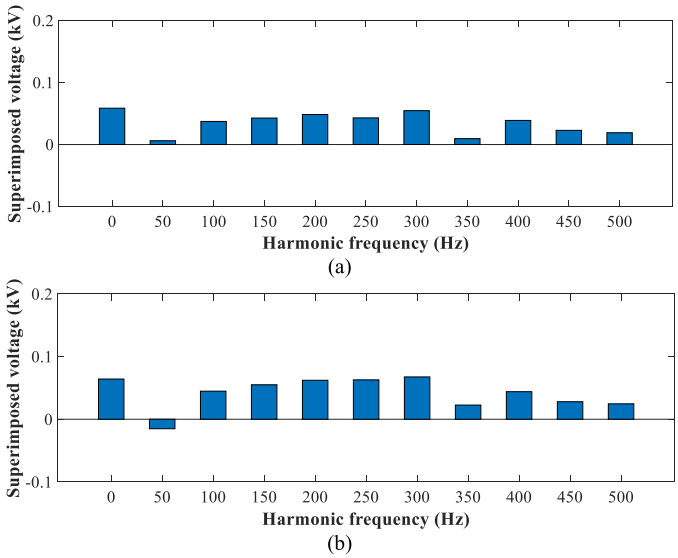

Fig. 3. Superimposed voltage harmonic spectra of phase a for the islanding events. (a) Event 1. (b) Event 2.

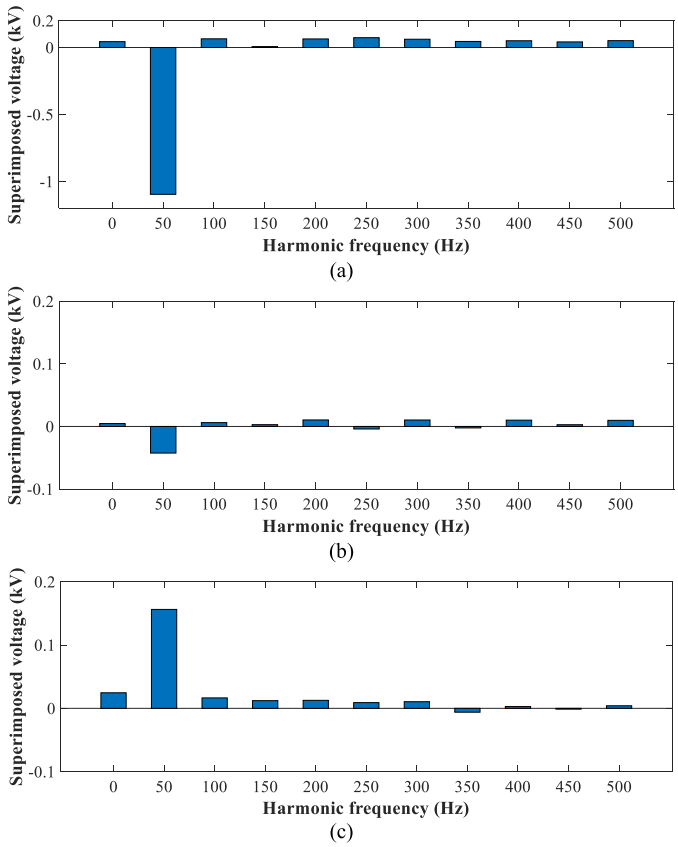

Fig. 4. Superimposed voltage harmonic spectra of phase a for the nonislanding events. (a) Event 3. (b) Event 4. (c) event 5.

should be emphasized that when a change occurs in the system, different behaviors may be observed due to the nonlinear nature of some devices in the distribution network. Hence, to overcome the challenge of islanding detection, a machine-learning-based

approach seems helpful to deal with the power system's complex situations.

III. Proposed Islanding Detection Scheme

Based on the discussions and analysis results of Section II, the proposed method uses the superimposed harmonic spectra of the three phases' voltage signals as input features for islanding detection. However, using full spectra and multiple input features makes it challenging to define and adjust thresholds as deployed in [22], [23], and [24] and express relationships analytically. On the other hand, complicated behaviors may be observed due to the nonlinear nature of network devices. Hence, to overcome these challenges, a machine-learning-based one-class classifier is employed for exploiting helpful information and decision-making based on the superimposed voltage harmonic spectra of the three phases. This classifier is first prepared through an offline process. Then, it is executed in real-time to detect islanding events. This method uses voltage signals sampled at a low rate according to the IEC 61850 Sampled Value standard to facilitate real-time implementation.

A. Offline Preparation

In the one-class classification problem, there is only one target class. Therefore, the one-class classifier should accurately describe the target training set and recognize that each new input pattern belongs to the target class or is an outlier [28]. In this article, the islanding condition is the target class, and other normal/non-islanding (e.g., faults, load change, and grid frequency and voltage fluctuations) conditions are considered outliers. The following main steps should be performed to prepare the one-class classifier:

Step 1: The target training set (i.e., T_1, T_2, T_3 … T_M) is generated by simulating M different islanding conditions in the system. For generating the ith target training pattern, T_i, data-windows, including the cycles before and after the ith islanding event occurrence time, are selected from the three-phase voltage signals measured at the PoC. The superimposed harmonic spectra are then extracted for each phase by applying the DFT, as shown in Fig. 1. Let us suppose that f_b and f_s are the system's fundamental and sampling frequencies, respectively. In that case, T_i is a vector that includes $3(\frac{f_s}{2f_b}+1)$ features (i.e., superimposed voltage harmonic magnitudes), considering the discrete harmonic frequencies from 0 Hz to f_s/2 for each phase. f_s is set as a multiple of $2f_b$.

Step 2: There are several one-class classifiers. The k-MDD classifier is deployed in this article for real-time islanding detection due to its simplicity and relatively low computational burden [28], [29]. In order to prepare this classifier, the target training set is optimally partitioned into k clusters (i.e., subsets) based on the iterative k-means clustering algorithm [30], [31]. The centroids of the resulting k optimal clusters (i.e., C_1^*, C_2^*, C_3^* … C_k^*) are stored as the prototype vectors.

Step 3: A threshold value is calculated as follows:

$$\delta_{\text{thr}} = \max_i \min_j \left\|T_i - C_j^*\right\|^2 \tag{1}$$

where $\|.\|$ denotes the Euclidean distance, C_j^* indicates the centroid (i.e., prototype vector) of the jth optimal cluster, and δ_{thr} is the threshold. As can be comprehended from (1), the threshold is equal to the maximum squared distance between the target training patterns and their nearest cluster centroids.

B. Real-Time Execution

When a new pattern, X, is presented to the prepared k-MDD classifier, its squared Euclidean distance to the nearest stored centroid (i.e., prototype vector) is calculated as follows:

$$\delta = \min_j \left\|X - C_j^*\right\|^2. \tag{2}$$

This squared distance, δ, should be compared with the threshold value δ_{thr} in order to make the decision

$$\begin{array}{l} X \in \text{ Target class if } \delta \le \delta_{\text{thr}} \\ X \notin \text{ Target class if } \delta > \delta_{\text{thr}} \end{array}. \tag{3}$$

It is common in power system protection algorithms to apply half-cycle or full-cycle DFT on measured current and voltage signals, depending on the protection requirements like speed and accuracy [32]. The harmonic spectrum in our article is extracted by applying the full-cycle DFT to the sampled voltage signal, which has been well presented in [33]. In the real-time application, at each time t, the superimposed spectra are extracted by applying the DFT, as shown in Fig. 1, considering two-cycle data-windows of the three-phase voltage signals measured at the PoC. The input pattern (i.e., feature vector) is then formed based on the superimposed voltage harmonic magnitudes of the three phases from 0 Hz to f_s/2. For example, with a sampling rate of 1000 samples per second or $f_s = 1$ kHz, the extractable harmonics include 0–500 Hz. This input pattern is presented to the prepared k-MDD classifier for the sake of decision-making based on (2) and (3). After detecting an islanding condition, the islanding detection logic signal changes from 0 to 1 and settles till being reset. Fig. 5 illustrates how the proposed scheme works in a real-time manner.

C. Adjusting the Number of Clusters

According to Section III-A, the only parameter that needs to be adjusted in the proposed scheme is the number of clusters, k. It is relatively simple to set this as an integer ranging from 1 to M. This parameter can be set by trial and error, too. However, a systematic validation process might lead to a more dependable setting.

For adjusting k through the validation process, a limited number of validation signals should be generated. This can be attained by simulating the system under different islanding and non-islanding conditions. For each possible value of k, the second and third steps described in Section III-A must be performed. The validation signals are then inputted into the prepared k-MDD classifier. After which, the percentage of validation loss for that value of k is calculated as follows:

$$VL = \frac{FN_V + FP_V}{N_V} \times 100 \tag{4}$$

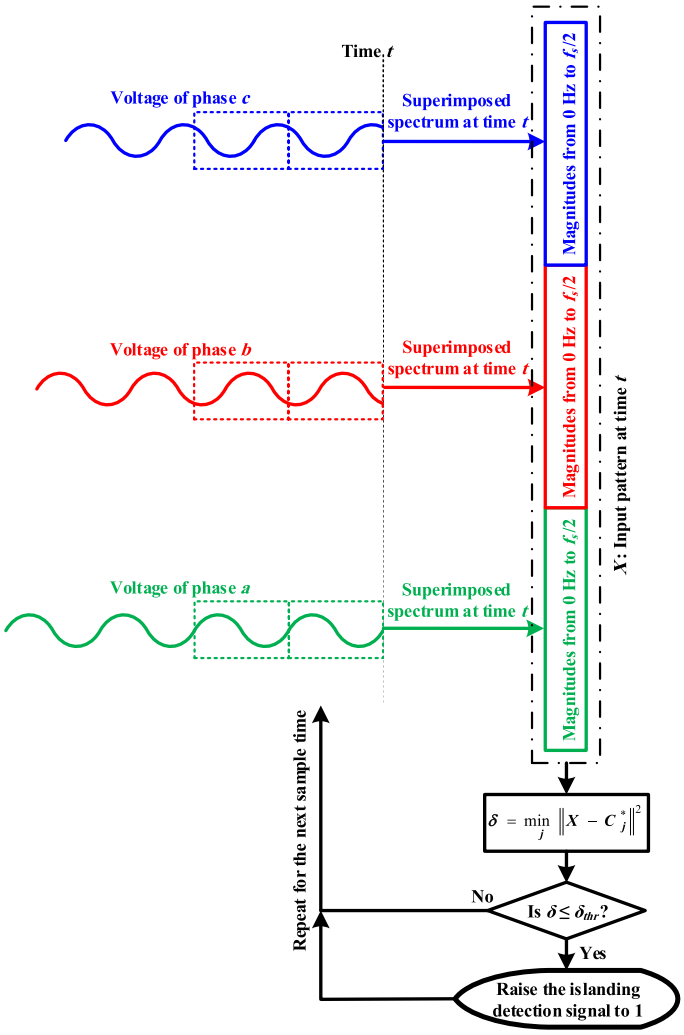

Fig. 5. Proposed islanding detection scheme in the real-time application.

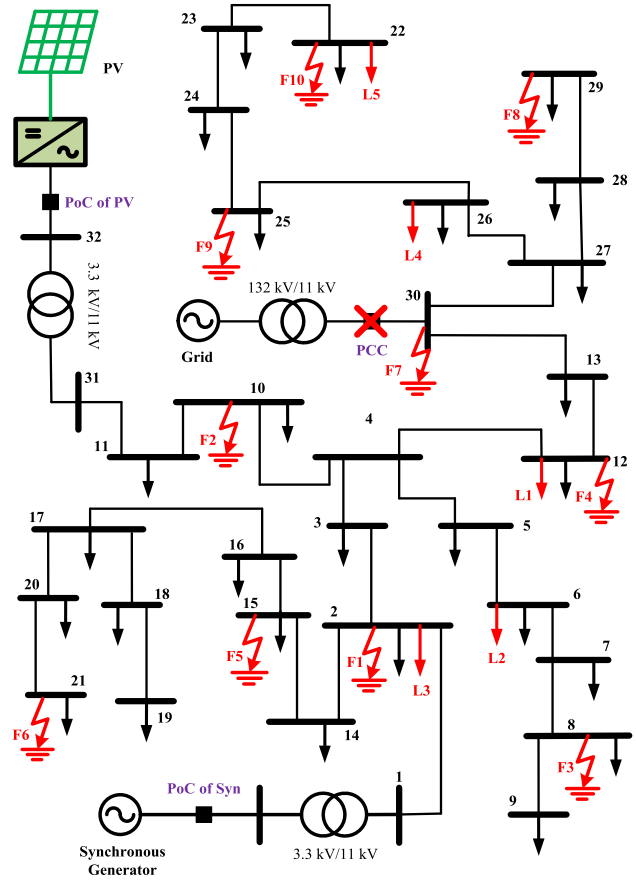

Fig. 6. Test MG.

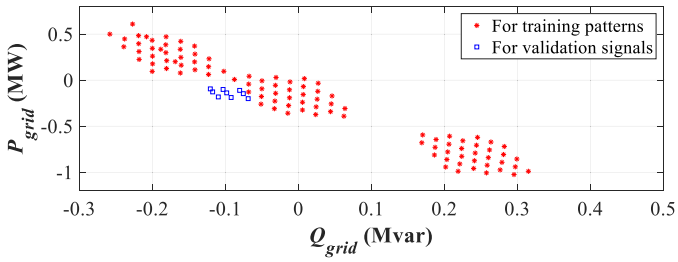

Fig. 7. Active and reactive powers injected from the grid before islanding events simulated for generating training patterns and validation signals.

where FN_V is the number of times the classifier has failed to detect islanding events, FP_V indicates the number of times the classifier has mal-operated under normal/non-islanding conditions, N_V is the total number of validation signals, and VL stands for the validation loss in percent. The value of k corresponding to the minimum validation loss is selected as the desired setting.

IV. Results and Discussions

The proposed scheme is programmed in MATLAB and examined in a typical test MG simulated in PSCAD/EMTDC.

A. Test System

The proposed islanding detection method is tested on a full-scale model of a segment of the Malaysian 11 kV distribution system [34]. The system comprises 32 buses, 27 lumped loads, a mini-hydro generator, and a PV generator, as illustrated in Fig. 6. The PV and mini-hydro generators operate at 3.3 kV. The mini-hydro generator has an inertia constant of 2.5 s. The PV and mini-hydro generators are linked to the distribution network through 2 MVA transformer units that step up the voltage level to 11 kV. The distribution network is connected to the grid via a 132 kV/11 kV transformer. The required voltage measurements for the proposed method are obtained at the PoC of PV (i.e., bus 32), with a sampling frequency of 1 kHz. The fundamental frequency of the system is 50 Hz.

B. Preparing a k-MDD Classifier

Following the first step described in Section III-A, the target training set is generated by simulating 100 islanding events in the test system under different pre-event conditions. Fig. 7 gives the active and reactive powers injected from the utility grid (i.e., P_{grid} and Q_{grid}) for these conditions. Considering the fundamental and sampling frequencies, the dimension of input

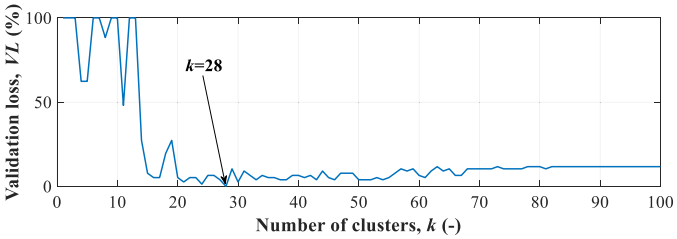

Fig. 8. Validation losses in terms of k.

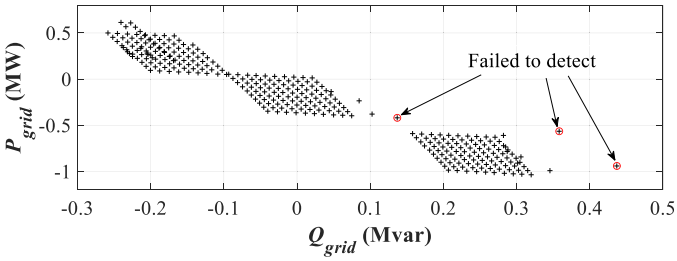

Fig. 9. Active and reactive powers injected from the grid before 320 islanding events simulated for tests.

feature vectors is 33 (as mentioned in Section III-A).For adjusting k, some validation signals are also generated by simulating nine islanding events and 68 non-islanding events using the test system with different conditions. The pre-event conditions for these islanding events are also indicated in Fig. 7. The conditions considered for the non-islanding ones are as follows.

1) Phase a-to-ground and three-phase-to-ground faults with fault resistances of 178 and 194 Ω at F1-F10 (as indicated in Fig. 6) lasted for 0.28 s (i.e., $2 \times 2 \times 10 = 40$ fault events)
2) Sudden connection of inductive loads with 0.44 and 0.395 MW active powers and 0.425 and 0.389 Mvar reactive powers at L1-L5 (as indicated in Fig. 6) (i.e., $2 \times 2 \times 5 = 20$ load change events)
3) Temporary changes in the grid's voltage by 17%, 15.5%, −17%, and −19% lasted for 0.35 and 0.38 s (i.e., $4 \times 2 = 8$ voltage change events)

For each integer value of k ranging from 1 to 100, a k-MDD classifier is prepared based on the second and third steps described in Section III-A and evaluated using the validation signals. Fig. 8 shows the obtained validation losses in terms of k. This figure indicates that $k = 28$ is the best adjustment since it results in a zero validation loss. Therefore, the k-MDD classifier with this optimal setting is considered for the test stage. This classifier's threshold value calculated based on (1) equals 621.0499 V^2.

C. Islanding Detection Tests

A total of 320 islanding events are simulated in the test system with pre-event P_{grid} and Q_{grid} given in Fig. 9.

The evaluation results confirm that the proposed scheme detects 317 out of 320 islanding events with a time delay in the range of 10–21 ms. In other words, the proposed method has a detection accuracy of about 99.06%, while it is fast enough

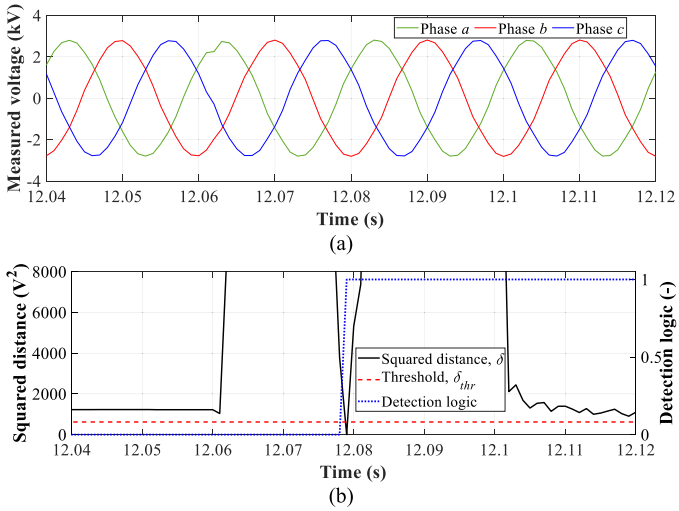

Fig. 10. Islanding event at 12.06 s when $P_{\text{grid}} = 0.609$ MW and $Q_{\text{grid}} = -0.227$ Mvar. (a) Measured voltage. (b) Squared distance and detection logic.

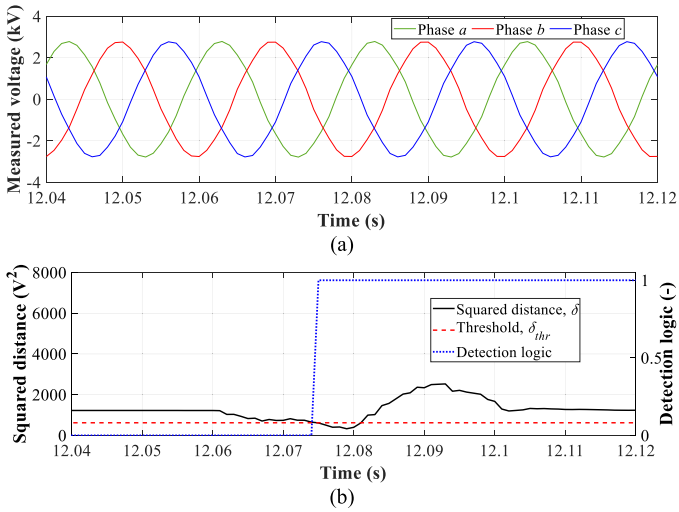

Fig. 11. Islanding event at 12.06 s when $P_{\text{grid}} = 0.013$ MW and $Q_{\text{grid}} = 0.021$ Mvar. (a) Measured voltage. (b) Squared distance and detection logic.

to meet the standard requirements desirably. The undetected islanding events are also indicated in Fig. 9. By comparing Figs. 7 and 9, it can be understood that the conditions of these three undetected events are almost outside the range covered in the training stage. It implies that the coverage of possible ranges is essential when generating the target training set.

It should be noted that the proposed scheme has not malfunctioned during any of the normal conditions before the islanding events. In order to provide a better sense of the scheme's real-time performance, the voltage measured at the PoC of PV, the real-time variations of the squared Euclidean distance, and the islanding detection logic signal are presented in Figs. 10 and 11 for two different islanding events at 12.06 s. As can be observed from these figures, the islanding events at 12.06 s are not visually recognizable in the voltage signals measured at the PoC of PV, especially in Fig. 11(a), with a low level of power mismatch with

TABLE I
ISLANDING DETECTION TEST RESULTS FOR DIFFERENT SNRS

SNR (dB)	Number of test cases	Detection accuracy (%)	Minimum delay (ms)	Maximum delay (ms)
∞	320	99.06	10	21
70	320	99.06	10	21
65	320	98.44	10	21
60	320	98.13	10	21
55	320	96.56	10	21
50	320	78.75	7	21

the utility grid. However, the proposed scheme has detected them based on the voltage's harmonic signature.

D. Effect of Measurement Noise

Different levels of white Gaussian noise are added to the three-phase voltage signals measured in 320 test cases of Section IV-C, while the prepared k-MDD classifier remains as before (i.e., trained based on the noiseless condition). The islanding detection test results for various signal-to-noise ratios (SNRs) are given in Table I for comparison. As seen from this table, the proposed islanding detection scheme can tolerate noisy signals even with an SNR of 55 dB, sacrificing 2.5% in its detection accuracy compared to the noiseless condition (infinite SNR). However, a noisy condition with an SNR of 50 dB significantly reduces the method's accuracy. It may be possible to improve the proposed scheme's performance in such a case via a filtering or preprocessing stage. It is worth noting that in the noisy conditions of Table I, the scheme has not malfunctioned during any of the normal conditions before the islanding events. Moreover, the minimum and maximum detection delays have remained unchanged, except for the SNR of 50 dB, due to the relatively higher level and unpredictable effect of random noise.

E. Stability During Short-Circuit Faults

Phase a-to-ground, phase c-to-ground, and three-phase-to-ground faults are applied at F1-F10 (as indicated in Fig. 6) with fault resistances of 0, 50, 100, and 200 Ω and lasted for 0.2 and 0.4 s, resulting in a total of 240 fault events. The test results show that the prepared k-MDD classifier remains stable before, during, and after all these fault events.

As an example of this correct performance, Fig. 12 shows the voltage measured at the PoC of PV, the real-time variations of the squared Euclidean distance, and the islanding detection logic signal for a solid three-phase-to-ground fault at 12.1 s at F6 that lasted for 0.4 s. It is evident from the figure that the proposed scheme did not malfunction, as δ has never been equal to or lower than δ_{thr}.

F. Stability Against Load Changes

Inductive loads with 0.045, 0.09, 0.135, 0.18, 0.225, 0.27, 0.315, 0.36, 0.405, and 0.45 MW active powers and 0.045, 0.09, 0.135, 0.18, 0.225, 0.27, 0.315, 0.36, 0.405, and 0.45 Mvar reactive powers are suddenly connected at L1-L5 (see Fig. 6) (i.e., $10 \times 10 \times 5 = 500$ load change events). The test results confirm that none of these load change events cause any

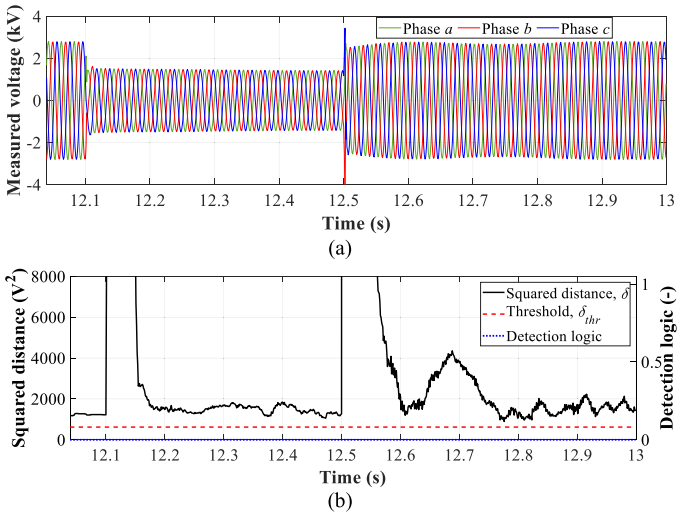

Fig. 12. Solid three-phase-to-ground fault at 12.1 s at F6 lasted for 0.4 s. (a) Measured voltage. (b) Squared distance, and detection logic.

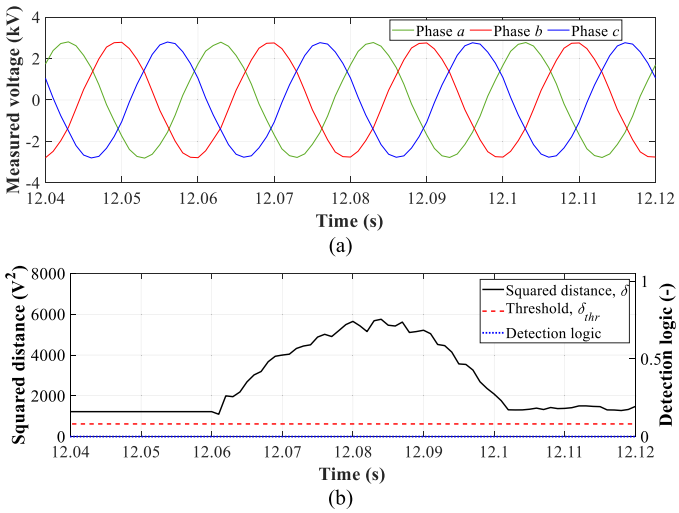

Fig. 13. Connection of a load (0.45 MW and 0.45 Mvar) at 12.06 s at L5. (a) Measured voltage. (b) Squared distance and detection logic.

malfunction to the prepared classifier. For instance, the test result is presented in Fig. 13 for the sudden connection of an inductive load with 0.45 MW active power and 0.45 Mvar reactive power at 12.06 s at L5. Whereas the load connection's effect is not visually recognizable in the voltage measured at the PoC of PV, this event temporarily changes the voltage's harmonic content. The proposed method has remained stable against it since δ has remained above δ_{thr}.

For further investigation, inductive single-phase loads with 0.395 and 0.44 MW active powers and 0.389 and 0.425 Mvar reactive powers are suddenly connected at L1, L3, and L5 (i.e., $2 \times 2 \times 3 = 12$ single-phase load change events). The test results verify that the proposed scheme can also remain stable in the case of these single-phase load change events.

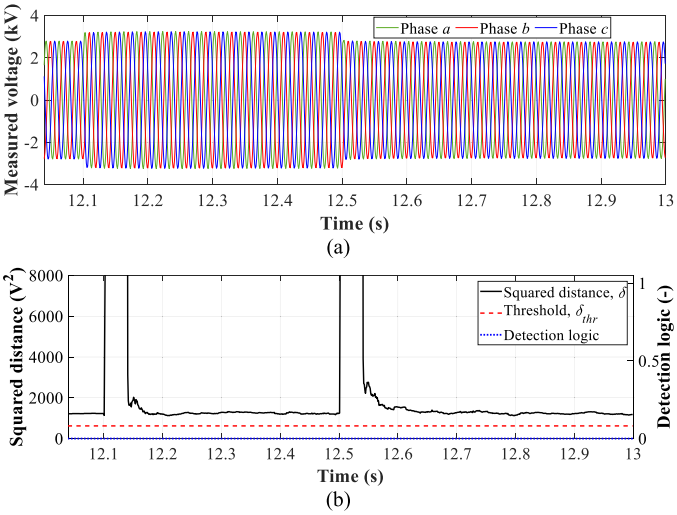

Fig. 14. Increase in the grid's voltage by 18% at 12.1 s lasted for 0.4 s. (a) Measured voltage. (b) Squared distance, and detection logic.

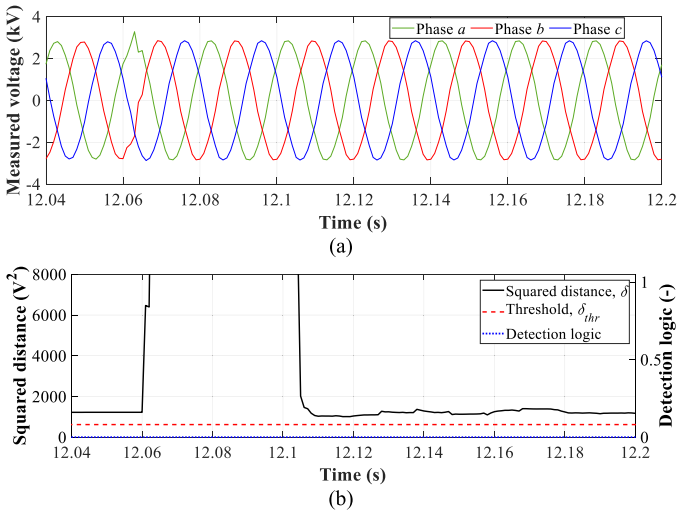

Fig. 15. Switching a capacitor bank with 0.45 Mvar reactive power at 12.06 s at L2. (a) Measured voltage. (b) Squared distance, and detection logic.

G. Stability During Grid's Voltage Changes

The grid's voltage magnitude is temporarily changed by 18%, 14%, 11%, 7%, −7%, −11%, −14%, and −18% lasting for 0.05, 0.1, 0.15, 0.2, 0.25, 0.3, 0.35, and 0.4 s (i.e., $8 \times 8 = 64$ voltage change events). The evaluation results confirm that the prepared k-MDD classifier remains stable before, during, and after all these temporary voltages' fluctuation events. As an example of the classifier's correct performance, the test result is presented in Fig. 14 for an increase in the grid's voltage magnitude by 18% at 12.1 s lasted for 0.4 s. It is clear that δ has always been greater than δ_{thr}, and the scheme has not malfunctioned.

H. Stability Against Capacitor Switching

Capacitor banks with 0.045, 0.09, 0.135, 0.18, 0.225, 0.27, 0.315, 0.36, 0.405, and 0.45 Mvar reactive powers are switched at L1-L5 (see Fig. 6) (i.e., $10 \times 5 = 50$ capacitor switching events). The assessment results show that none of these events cause the prepared k-MDD classifier to mal-operate. For instance, the test result is presented in Fig. 15 for switching a capacitor bank with 0.45 Mvar reactive power at 12.06 s at L2. As is apparent from this figure, the scheme has not mal-operated during the temporary transients after the capacitor switching event since δ has remained above δ_{thr}.

I. Stability During Grid's Frequency Changes

The grid's frequency is temporarily changed by 2, 1.5, 1, 0.5, −0.5, −1, −1.5, and −2 Hz, lasting for 0.05, 0.1, 0.15, 0.2, 0.25, 0.3, 0.35, and 0.4 s (i.e., $8 \times 8 = 64$ frequency change events). The test results confirm that the proposed scheme remains stable before, during, and after all these frequency change events. As an example of the scheme's stability, the test result is presented in Fig. 16 for an increase in the grid's frequency by 2 Hz at 12.06 s lasted for 0.4 s. While it is difficult to visually recognize this frequency change in the voltage measured at the PoC of PV, its effect on the extracted harmonic spectra is observable in the

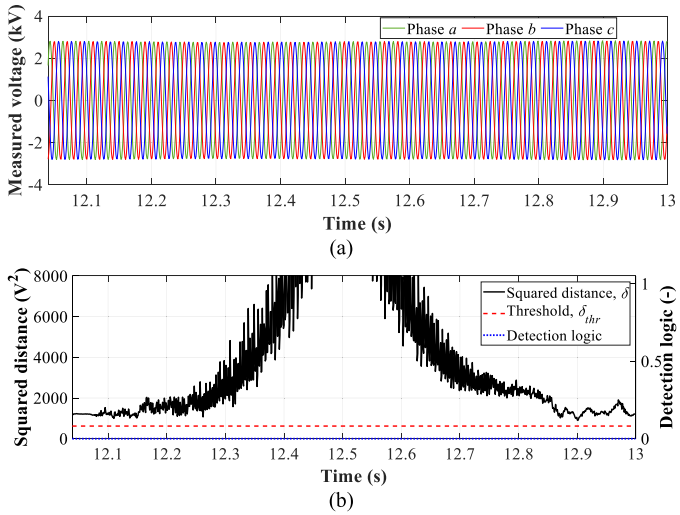

Fig. 16. An increase in the grid's frequency by 2 Hz at 12.06 s lasted for 0.4 s. (a) Measured voltage. (b) Squared distance, and detection logic.

real-time variations of δ. As comprehendible from this figure, δ has always remained above δ_{thr}, preventing misidentification.

J. Impact of Nonlinear/Harmonic Loads

A portion of the load in the test MG shown in Fig. 6 is replaced with an inductive-resistive 0.1 MW harmonic load with a power factor of 0.85. This new harmonic load generates third, fifth, and seventh harmonic currents. It is worth mentioning that according to the IEEE Std. 519-2014, the maximum THD, which can be applied at the PCC or PoC for the voltage level of more than 1 kV until 69 kV should not exceed 5%. It has been mentioned that system owners or operators should limit line-to-neutral voltage harmonic at the PCC or PoC.

Therefore, the new harmonic load generates third, fifth, and seventh harmonic currents with magnitudes of 50%, 25%, and 15% of the fundamental current magnitude, respectively. This substantial harmonic load, which has not been considered in the

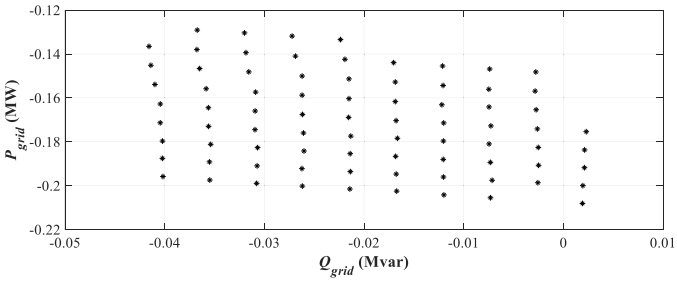

Fig. 17. Active and reactive powers injected from the grid before 80 islanding events simulated in the presence of the unseen harmonic load.

TABLE II
COMPARISON TO OTHER ISLANDING DETECTION METHODS

Ref. No.	Methodology	Detection time (s)	Measured signals	Accuracy
[22]	Change of 5th harmonic voltage magnitude	0.308	V_{abc}	NDZ: -5.9%<ΔP<4.1% -17.3%<ΔQ<29.1%
[23]	Change of selected harmonic distortion	0.070	V_{abc}	91.6%
[24]	A combination of voltage unbalance and total harmonic distortion detection and bilateral reactive power variation	0.300	V_{abc} & I_{abc}	NDZ is eliminated
[25]	A combination of slantlet transform and ridgelet probabilistic neural network	0.17	V_{abc}, f, df/dt, dV/dt, dV_d/dt, dV_q/dt & *dc-link voltage*	100% without noise
[26]	A combination of a signal processing approach and support vector machine	0.04	f, P, Q, RMS_I, RMS_V, THD_I, and THD_V	NDZ: 9.52%
Proposed method	Harmonic signature-based one-class classifier	0.021	V_{abc}	99.06%

training stage, is connected to bus 11, very close to the measuring point (i.e., the PoC of PV) to study the impact of the harmonic sources. For evaluating the detection accuracy in the presence of the unseen harmonic load, 80 islanding events are simulated with pre-event P_{grid} and Q_{grid} given in Fig. 17.

The test results reveal that the proposed scheme detects 65 out of these islanding events (i.e., the detection accuracy of 81.25%) with a time delay in the range of 63–960 ms. Although the new harmonic load has somewhat degraded the scheme's detection accuracy and speed, the results are promising since this substantial harmonic load has not been included in the training patterns' generation conditions.

K. Comparison

Table II compares the distinctive aspect of the proposed islanding detection technique with similar methods, which use harmonic contents or a combination of signal processing and machine-learning approaches. The points selected for comparison in this table are the methodology, detection time, measured signals, and accuracy. According to Table II, the proposed scheme has the lowest detection time. Furthermore, unlike the techniques introduced in [24], [25], and [26], the proposed islanding detection method only relies on the voltage measurement at the PoC of DERs. In other words, it does not require other parameters such as current, frequency, active power, and reactive power or their derivatives. As a result, the proposed method is immune to corresponding errors and issues like current transformer saturation or high sensitivity to noise. Although the strategies presented in [22] and [23] also need only the voltage measurement, Table II gives that the proposed method's NDZ and accuracy have been significantly improved compared to them.

V. CONCLUSION

This article proposed an intelligent islanding detection scheme that relies on voltage harmonic signatures and a *k*-MDD classifier. In order to test the performance of the proposed strategy, the simulations under several scenarios were conducted in a typical test MG with synchronous and inverter-based DERs. According to the test results, the proposed method demonstrated satisfactory accuracy and detection time for different islanding events. Furthermore, our proposed method remained stable in various situations, including normal operations, short-circuit faults, load changes, voltage changes, capacitor switching, and frequency changes. In addition to its desirable accuracy, detection time, and stability, the proposed method is inherently immune to current transformer errors, communication channel failures, and data synchronization errors and compatible with distributed and decentralized control strategies as it relies only on measuring the three-phase voltage signals at the PoC of DERs. Moreover, the proposed method works fine with low sampling frequency, making it compatible with most existing infrastructures.

Under perfectly matched loading conditions, the voltage signals measured at the PoC of DERs may remain unchanged during an islanding event, showing no distinct or noticeable variations. In other words, in these exceptional cases, the method may not identify an islanding event based on passive voltage measurements alone. This problem can be focused on in future studies.

REFERENCES

[1] M. Seyedi, S. A. Taher, B. Ganji, and J. Guerrero, "A hybrid islanding detection method based on the rates of changes in voltage and active power for the multi-inverter systems," *IEEE Trans. Smart Grid,* vol. 12, no. 4, pp. 2800–2811, Jul. 2021.

[2] M. Karimi et al., "An islanding detection technique for inverter-based distributed generation in microgrids," *Energies 14*, vol. 130, no. 1, pp. 1–18, Jan. 2021, doi: 10.3390/en14010130.

[3] S. F. Zarei, H. Mokhtari, and F. Blaabjerg, "Fault detection and protection strategy for islanded inverter-based microgrids," *IEEE Trans. Emerg. Sel. Topics Power Electron.,* vol. 9, no. 1, pp. 472–484, Feb. 2021.

[4] R. Bakhshi-Jafarabadi and J. Sadeh, "New voltage feedback-based islanding detection method for grid-connected photovoltaic systems of microgrid with zero non-detection zone," *Int. Eng. Technol. Renew. Power Gener.,* vol. 14, pp. 1710–1719, Jul. 2020.

[5] *IEEE Standard for Interconnection and Interoperability of Distributed Energy Resources with Associated Electric Power Systems Interfaces*, IEEE Std 1547-2018 (Revision of IEEE Std 1547-2003), 2018.

[6] "Operability strategy report 2021," National Grid ESO, London, U.K., Dec. 2020. [Online]. Available: https://www.nationalgrideso.com/document/183556/download

[7] G. Bayrak and E. Kabalci, "Implementation of a new remote islanding detection method for wind–solar hybrid power plants," *Renew. Sust. Energy Rev.,* vol. 58, pp. 1–15, May 2016.

[8] R. Bekhradian, M. Davarpanah, and M. Sanaye-Pasand, "Novel approach for secure islanding detection in synchronous generator based microgrids," *IEEE Trans. Power Del.,* vol. 34, no. 2, pp. 457–466, Apr. 2019.

[9] R. M. R., A. Sankar and S. R, "Synchrophasor data driven islanding detection, localization and prediction for microgrid using energy operator," *IEEE Trans. Power Syst.,* vol. 36, no. 5, pp. 4052–4065, Sep. 2021.

[10] A. Khamis et al., "A review of islanding detection techniques for renewable distributed generation systems," *Renew. Sust. Energy Rev.,* vol. 28, pp. 483–493, Dec. 2013.

[11] S. Nikolovski, H. R. Baghaee, and D. Mlakić, "Islanding detection of synchronous generator-based DGs using rate of change of reactive power," *IEEE Syst. J.,* vol. 13, no. 4, pp. 4344–4354, Dec. 2019.

[12] A. G. Abd-Elkader et al., "A passive islanding detection strategy for multi-distributed generations," *Int. J. Elect. Power Energy Syst.*, vol. 99, pp. 146–155, Jul. 2018.

[13] M. A. Farhan and K. S. Swarup, "Mathematical morphology-based islanding detection for distributed generation," *Int. Eng. Technol. Gener. Transmiss. Distrib.*, vol. 10, pp. 518–525, Feb. 2016.

[14] R. Zamani et al., "A novel synchronous DGs islanding detection method based on online dynamic features extraction," *Elect. Power Syst. Res.*, vol. 195, Jun. 2021, Art. no. 107180.

[15] P. K. Ganivada and P. Jena, "Active slip frequency based islanding detection technique for grid-tied inverters," *IEEE Trans. Ind. Inform.*, vol. 16, no. 7, pp. 4615–4626, Jul. 2020.

[16] D. Sivadas and K. Vasudevan, "An active islanding detection strategy with zero nondetection zone for operation in single and multiple inverter mode using GPS synchronized pattern," *IEEE Trans. Ind. Electron.*, vol. 67, no. 7, pp. 5554–5564, Jul. 2020.

[17] C. N. Papadimitriou, V. A. Kleftakis, and N. D. Hatziargyriou, "A novel method for islanding detection in dc networks," *IEEE Trans. Sustain. Energy*, vol. 8, no. 1, pp. 441–448, Jan. 2017.

[18] A. Rostami, A. Jalilian, S. Zabihi, J. Olamaei, and E. Pouresmaeil, "Islanding detection of distributed generation based on parallel inductive impedance switching," *IEEE Syst. J.*, vol. 14, no. 1, pp. 813–823, Mar. 2020.

[19] X. Chen, Y. Li, and P. Crossley, "A novel hybrid islanding detection method for grid-connected microgrids with multiple inverter-based distributed generators based on adaptive reactive power disturbance and passive criteria," *IEEE Trans. Power Electron.*, vol. 34, no. 9, pp. 9342–9356, Sep. 2019.

[20] Y. M. Makwana et al., "Auto-correlation-based Islanding detection technique verified through hardware-in-loop testing," *Int. Eng. Technol. Gener. Transmiss. Distrib.*, vol. 13, pp. 3792–3802, Sep. 2019.

[21] W.-M. Lin, C.-H. Wu, C.-H. Lin, and F.-S. Cheng, "Detection and classification of multiple power-quality disturbances with wavelet multiclass SVM," *IEEE Trans. Power Del.*, vol. 23, no. 4, pp. 2575–2582, Oct. 2008.

[22] J. Merino, P. Mendoza-Araya, G. Venkataramanan, and M. Baysal, "Islanding detection in microgrids using harmonic signatures," *IEEE Trans. Power Del.*, vol. 30, no. 5, pp. 2102–2109, Oct. 2015.

[23] R. Haider et al., "Harmonic-signature-based islanding detection in grid-connected distributed generation systems using Kalman filter," *Int. Eng. Technol. Renew. Power Gener.*, vol. 12, pp. 1813–1822, Nov. 2018.

[24] G. Wang et al., "Design consideration and performance analysis of a hybrid islanding detection method combining voltage unbalance/total harmonic distortion and bilateral reactive power variation," *CPSS Trans. Power Electron. Appl.*, vol. 5, pp. 86–100, Mar. 2020.

[25] M. Ahmadipour et al., "Islanding detection technique using slantlet transform and ridgelet probabilistic neural network in grid-connected photovoltaic system," *Appl. Energy*, vol. 231, pp. 645–659, Dec. 2018.

[26] H. R. Baghaee, D. Mlakić, S. Nikolovski, and T. Dragičcvić, "Anti-islanding protection of PV-based microgrids consisting of PHEVs using SVMs," *IEEE Trans. Smart Grid*, vol. 11, no. 1, pp. 483–500, Jan. 2020.

[27] X. Kong et al., "Deep learning hybrid method for islanding detection in distributed generation," *Appl. Energy*, vol. 210, pp. 776–785, Jan. 2018.

[28] D. M. J. Tax, "One-class classification: Concept-learning in the absence of counter-examples," Ph.D. dissertation, Delft Univ. Technol., Delft, Netherlands, 2001.

[29] A. Bánhalmi et al., "A one-class classification approach for protein sequences and structures," in *Proc. Int. Symp. Bioinf. Res. Appl.*, 2009, pp. 310–322.

[30] R. Xu and D. Wunsch, *Clustering*. Hoboken, NJ, USA: Wiley, 2009.

[31] *MATLAB User's Guide: R2020b Documentation*. Natick, MA, USA: MathWorks, 2020.

[32] Q.-H. Wu et al., *Protective Relaying of Power Systems Using Mathematical Morphology*. Berlin, Germany: Springer, 2009.

[33] E. O. Brigham, *The Fast Fourier Transform*. Englewood Cliffs, NJ, USA: Prentice-Hall, 1974.

[34] N. A. Yusof et al., "A new under-voltage load shedding scheme for islanded distribution system based on voltage stability indices," *IEEJ Trans. Elect. Electron. Eng.*, vol. 12, pp. 665–675, 2017.